Journal of Engineering Science and Technology
8th EURECA 2017 Special Issue August (2018) 67 - 78

A NUMERICAL ASSESSMENT OF MICROTOPOGRAPHIES WITH VARIED GEOMETRIES IN RELATION TO BIOFOULING CONTROL

FELICIA WONG YEN MYAN[1,*], LAM KUO MIN[1],
LIM CHIN HONG[1], JAMES WALKER[2]

[1]School of Engineering, Taylor's University, Taylor's Lakeside Campus,
No. 1 Jalan Taylor's, 47500, Subang Jaya, Selangor DE, Malaysia
[2]Department of Civil Engineering, University of Nottingham Ningbo China,
199, Taikang East Road, Yinzhou District, Zhejiang Province, 315100, Ningbo, China
*Corresponding Author: feliciayenmyan.wong@taylors.edu.my

Abstract

Biofouling is the unwanted attachment of organisms and microorganisms to a submerged surface. It is a natural phenomenon that results in negative impacts on man-made industries such as the marine industry, food industry, water treatment among others. Studies have shown that the application of surface topography with varied geometries and sizes have the potential to prevent biofouling. This research aims to assess microtopographies of varied geometries and shape in relation to biofouling control. The size and dimensions of the topographies were kept the same at 150 µm. This research is computational where simulations of flow in three-dimensional (3D) models were performed with ANSYS Fluent, a Computational Fluid Dynamics (CFD) software. With the aid of CFD, simulations of fluid flow in 3D models that consist of surface topographies with varied geometries and defined boundary conditions were conducted. The topographies investigated include pillars, octagonals, cross shaped grooves and square grooves. Hydrodynamic variations of interest that were analysed upon completion of the simulations include wall shear stress and velocity. Analysis of simulations show that the presence of topographies disrupt uniform flow and creates hydrodynamic fluctuations that discourage biofouling settlement. Simulations indicate that the pillars topography would likely have the best antifouling potential because it is the least likely to result in the formation of many vortices and also because shear stresses at the peaks of this topography are the highest among the four investigated topographies.

Keywords: Antifouling, Biofouling control, Topography geometries, Wall shear stress.

1. Introduction

Biofouling is the unwanted attachment of organisms and microorganisms to a surface. It usually starts within minutes after a surface is in contact with water. Biofouling starts with the formation of biofilms, which include proteins, polysaccharides, both dead and living bacteria encased in extracellular polymeric substances (EPS) [1]. Biofilms may seem harmless, but it actually brings more harm than good affecting parts and systems of various industries. The cost of antifouling equipment for the oil and gas sector alone have been estimated to be USD 960 to 1280 million in the United States during 1982 [2]. To date, this amount could have escalated to billions of dollars. This illustrates the need to implement innovative methods and intensive research on the subject to prevent and mitigate biofouling.

Numerous approaches have been used to tackle biofouling with limited success. One of these approaches involved the use of toxic biocides such as Tributyltin (TBT) which was frequently used due to its high efficacy at deterring biofouling. However, this method has been eliminated and prohibited due to its detrimental effects on the environment [3].

Using copper-nickel alloys for ships and aquamarine structures mitigated biofouling to a degree but were not as effective in freshwater environments [4]. Over an extended period, biofouling may eventually build up anyway. Fortunately, there are also non-toxic alternative coatings used for antifouling applications, which are specially grouped and catered around specific performance requirements to provide optimal solutions to clients in the market nowadays. These coatings, often called foul release coatings, include silicone based coatings, hydrogel coatings, thermo-responsive hydrogel coatings and hydrolysis binder coatings [5]. Nevertheless, these coatings sold by companies like Pittsburgh Plate Glass (PPG) Industries are very costly.

Current research to develop new solutions for biofouling control aims to be non-toxic, requires little or no power consumption with small energy footprint, has a long lifecycle and requires low maintenance.

Aside from foul-release coatings, another non-toxic antifouling approach is the application of surface topography. Many studies have investigated surface topographies of various shapes and sizes in their efforts to reduce or prevent biofouling. The design, developments and fabrication of such surfaces usually require extensive lab experiments that can be time-consuming and costly.

This led to recent research, which applied Computational Fluid Dynamics (CFD) to assess the antifouling characteristics of microwell arrays arranged in a channel that was 1 mm in width and 0.11 mm in height [6]. The application of CFD is still a relatively new approach to understand the antifouling properties of a surface topography. Nonetheless, this approach is advantageous because it permits the analyses of flow characteristics over such surfaces. Such observations would otherwise be challenging to do with lab experiments or field tests.

The goal of this research is to study and assess microtopographies of varied geometries in relation to biofouling control. Larger magnitude of hydrodynamic variations (i.e., wall shear stress, velocity) creates higher hydrodynamic disturbance towards microorganisms and unwanted surface inhabitants, therefore exhibits better antifouling efficacy for biofouling control [7].

This paper presents results of CFD simulations carried out to compare and analyse hydrodynamic variations over microtopographies that are uniform in size but varied in geometry.

2. Methods

2.1. 3D Topography geometry modelling

3D models of patterned surfaces with varied microtopography geometries and fixed sizes were modelled utilizing the CAD software SOLIDWORKS 2015 Student Edition.

A study concluded that microtopography sizes of 64-256 µm significantly reduced cyprids settlements on a submerged surface [7]. It could be argued that 64-256 µm were too small to accommodate cyprids with body widths of 500 µm or larger. Sizes of 64 µm and below, however, promotes biofouling of cyprids, which might be due to its antennal discs (approximately 30 µm) being compatible with the topography size.

It is challenging to simulate dynamic conditions of a field test site especially with the presence of various types of microorganisms in the water. In addition to that, researchers and engineers have yet to determine a fixed optimum microtopography size that exhibits optimum antifouling efficacy. Thus to simplify and make simulations easier for this research, patterned surfaces with microtopography size of 150 µm (approximately average the size of 64-256 µm range) were chosen as a fixed size (constant variable) for all four models. It is again emphasized that the objective of this research places priority on varying the topography geometries.

Figure 1 shows the four models with different topography geometries, namely pillars, octagons, cross-shaped grooves and square grooves. All pillars and octagons have a diameter, height and distance apart of 150 µm with a 10×20 topography array. Squared grooves have a height, width and distance apart of 150 µm. However, each groove had a length of 2.85 mm so that it is equivalent in length to the pillar and octagon arrays.

The four geometries were chosen for this research due to its relation to studies that have been published by Petronis et al. [8] and Won et al. [9]. Their findings act as a good baseline for the author to achieve the objectives of this project.

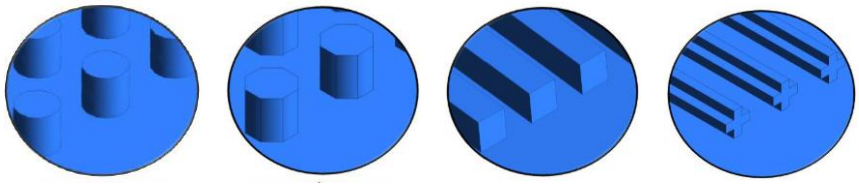

(a) 150 µm pillar model **(b) 150 µm octagon model** **(c) 150 µm squared groove model** **(d) 150 µm Cross-shaped groove model**

Fig. 1. The 3D models of the four different geometries that are investigated in this study.

2.2. Numerical setup

The CFD-software package ANSYS Fluent, version 18 was used for simulations in this study. The continuity equation, Eq. (1) and the Navier-Stokes equations, Eqs. (2) to (4) ensured the conservation of mass and momentum. The k-ω model was selected as the turbulence model for this research because it switches from the normal wall function to a low-Reynolds number formulation. This turbulence model is also suitable because it is commonly used for shear-driven flows and wall shear is a focus in this study.

$$\frac{\partial \rho}{\partial t} + \nabla \cdot (\rho V) = 0 \tag{1}$$

$$\frac{\partial \rho u}{\partial t} + \nabla \cdot \rho u V = -\frac{\partial \rho}{\partial x} + \nabla \cdot (\mu \nabla u) + S_{m,x} \tag{2}$$

$$\frac{\partial \rho v}{\partial t} + \nabla \cdot \rho v V = -\frac{\partial \rho}{\partial y} + \nabla \cdot (\mu \nabla v) + S_{m,y} \tag{3}$$

$$\frac{\partial \rho w}{\partial t} + \nabla \cdot \rho w V = -\frac{\partial \rho}{\partial z} + \nabla \cdot (\mu \nabla \mathrm{w}) + S_{m,z} \tag{4}$$

Fluid flow is modelled to be Newtonian and incompressible. The density ρ, and dynamic viscosity μ, of the fluid is 1000 kgms^{-3} and 0.001 kgm^{-1}s^{-1} respectively. The no-slip boundary condition was applied to the walls of the fluid domain. The mass-flow rate at the-inlet is 0.001 kgs^{-1}, while the outlet was set to outflow at x-direction.

2.3. Mesh convergence analysis

The 3D models were meshed with ANSYS Meshing. Figure 2 shows an example of the fluid domain model that is 8 mm in width and height, with a length of 80 mm. This fluid domain will be fixed in size for all four models.

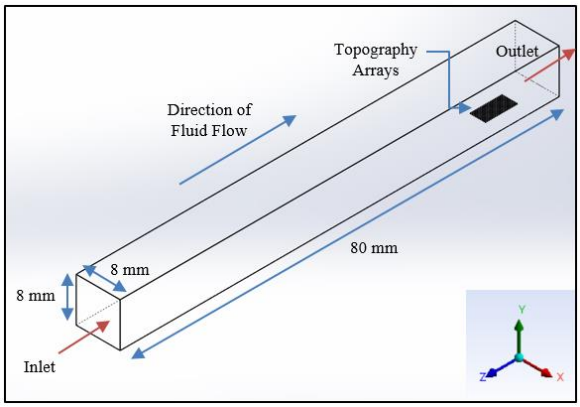

Fig. 2. 3D model of 150 µm pillar fluid domain with dimensions and topography placement.

According to Hagen-Poiseuille's Flow law, pressure drop will occur when an incompressible fluid flows through a channel with constant cross-section and a length longer than its diameter. Likewise, steady and laminar flow will be induced within such channel. Thus to ensure that the flow in this study is steady, laminar flow is fully induced and a good velocity profile is achieved, the length of the

channel is thus set at 80 mm for the channel to be long enough to avoid velocity interference at the inlet [10].

Figure 3 presents an example of a fully meshed fluid domain model and a zoomed-in topography array of 150 µm pillars with refined meshes. All four models were meshed with tetrahedral elements.

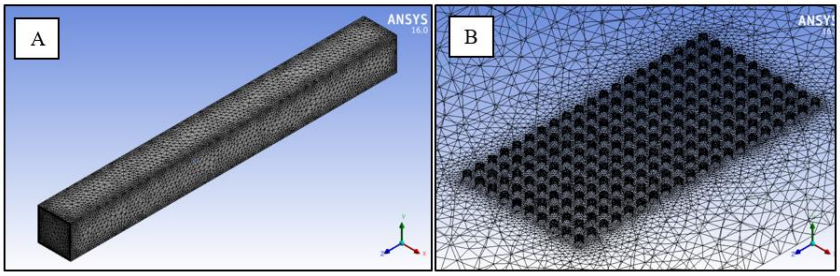

Fig. 3. (A) Fully meshed 150 µm pillar fluid domain model, (B) Refined meshes of 150 µm pillar topography array.

For every model, a mesh convergence analysis was performed to optimize the number of mesh elements. This method reduces computational time for simulations while maintaining the quality of the results. A study done by Halder et al. [11] refined mesh elements in consecutive models and performed respective simulations for each mesh refinements. Mesh convergence was considered satisfied when the difference of wall shear stress between each mesh refinements was less than 5%. The model with the least mesh elements and with a relative error percentage of less than 5% will then be chosen as the optimum model. Table 1 below presents the results of mesh convergence analysis for the four models.

Table 1. Mesh convergence analysis results

3D Model	Number of Elements (millions)	Relative Error (%)	Optimum Number of Elements (millions)
Pillars	0.92 →1.20	4.5	0.92
	1.20→1.84	3.7	
Octagons	0.32→0.45	12.9	0.45
	0.45→1.15	4.9	
Cross Shaped Grooves	0.36→1.42	9.3	1.42
	1.42→1.97	4.3	
Squared Grooves	0.25→0.43	8.6	0.43
	0.43→1.01	3.5	

2.4. Data acquisition

Figure 4 illustrates how velocity was measured for the pillar topography model. Average velocities were measured at the peaks of the topography arrays (red line) and at 30 µm above the base of the wall surface (blue line). Average velocities were also measured at similar positions for the remaining four topographies.

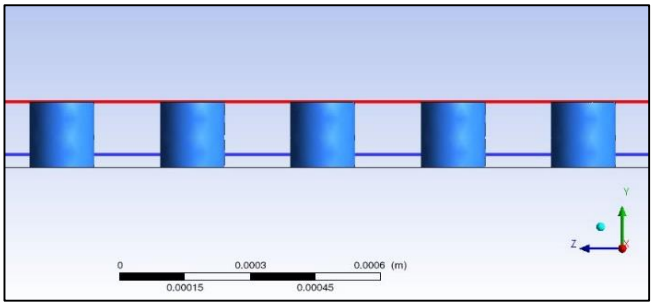

Fig. 4. Side view of pillar topography with red and blue lines where average velocity was measured.

Figure 5 illustrates how wall shear stress was measured for the pillar topography model. Average wall shear stresses were measured at the peaks of the topography arrays (red line) and at the base of the wall surface (orange line). Average wall shear stresses were also measured at exact positions for the other topographies.

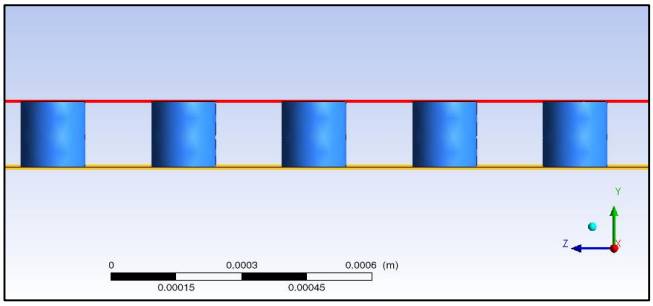

Fig. 5. Side view of pillar topography with red and orange lines where average wall shear stress was measured.

The positions were chosen at the peaks and base to calculate average wall shear stress because these are the positions that are experiencing the highest and the lowest shear stresses respectively. The average values for velocity and wall shear stress were calculated and compared between the various topography geometries.

3. Results and Discussion

This study aims to investigate the hydrodynamic fluctuations in the vicinity of topographies with varied geometries and suggest the topography with the best antifouling potential. The greater the fluctuations of the flow parameters (i.e., velocity, wall shear, etc.), the more "volatile" the flow is in a particular region, the more fluctuation the hydrodynamic disturbance towards microorganisms and unwanted surface inhabitants, therefore exhibit better antifouling efficacy for biofouling control.

The hydrodynamic variables that were analysed in this study were velocity and wall shear stress. Velocity streamlines represent how fluid flows inside the channel over the arrays of topography geometries whereas wall shear stress exhibits the shear stress induced by solid boundaries of the patterned surfaces.

3.1. Velocity

3.1.1. Velocity streamline profiles of topographies

Figure 6 shows the velocity streamline profiles of all the four topographies that are investigated in this study.

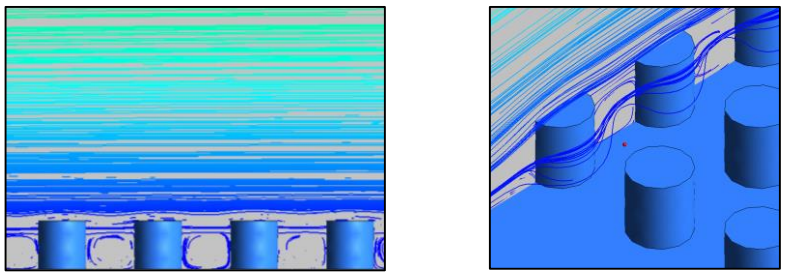

(a) Pillar topography

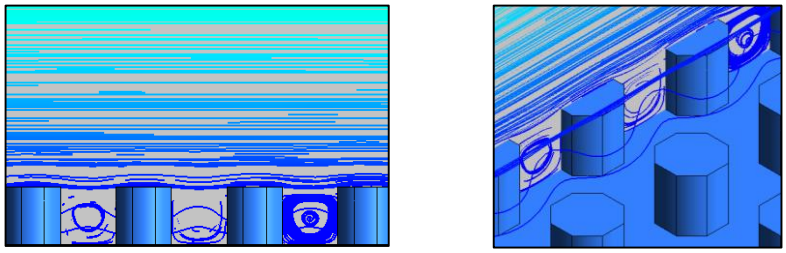

(b) Octagonal topography

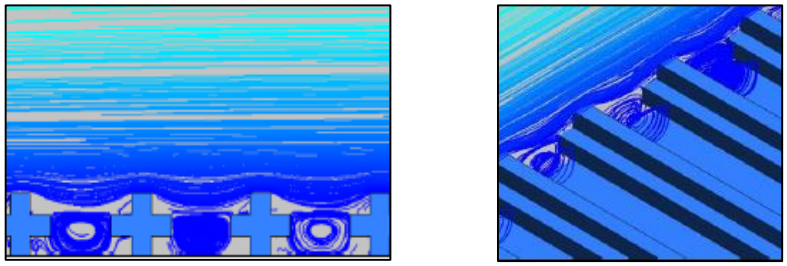

(c) Cross-shaped grooves

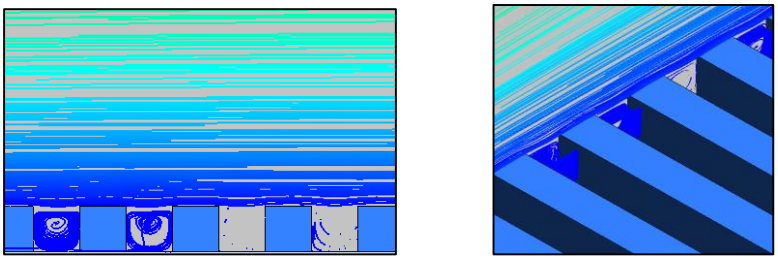

(d) **Square grooves**

Fig. 6. Velocity streamline profiles for all four topographies from the side view (figure on the left) and the isometric view (figure on the right.)

Vortices were found to form intermittently between gaps or amongst the patterns for all four topographies. These vortices are indicative of flow circulation between the patterns. However, several studies have suggested that these vortices could aid in the accumulation of biofouling material and should be minimised if possible [12]. Figure 6 also shows that the formation of vortices are more consistently between the gaps of both the cross and square grooves. This suggests that both these topographies would be less suited for biofouling control in comparison to the pillar and octagonal topographies.

3.1.2. Average velocity

Figure 7 summarizes the average velocity at the peaks and at 30 µm above the base of all topographies.

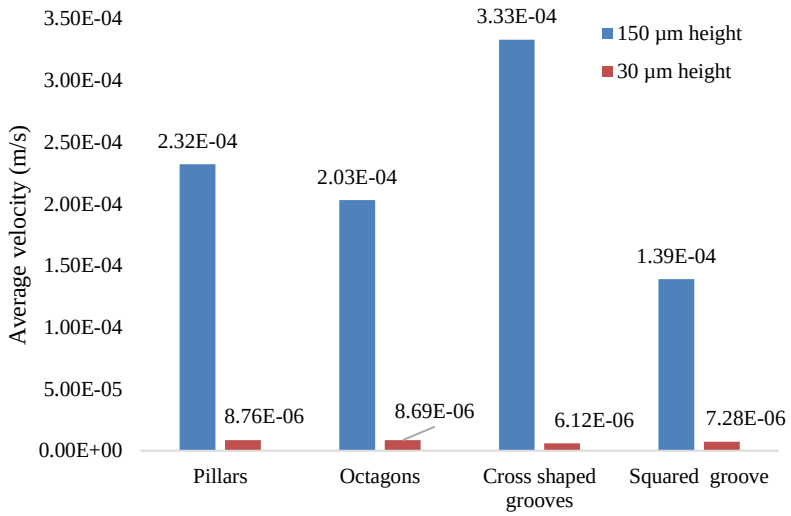

Fig. 7. Average velocities at 150 µm peaks and 30 µm above base surface for all 4 topographies.

The histogram shows that cross shaped grooves have the highest average velocities at the peak, followed by pillars, octagons and lastly squared grooves. Average velocities at 30 µm heights only show slight differences between all four topographies.

For all topography geometries, the average velocity at 150 µm height is at least 19 times greater than average velocity at the 30 µm height. This is because the topographies are hurdles towards fluid flow, which significantly reduces flow velocities. The nearer the distance towards the base, the lower the fluid velocity until it reaches 0 m/s at base Y=0.

3.2. Wall shear stress

Figure 8 shows the contour plot of wall shear stress exerted on pillar topography in isometric view.

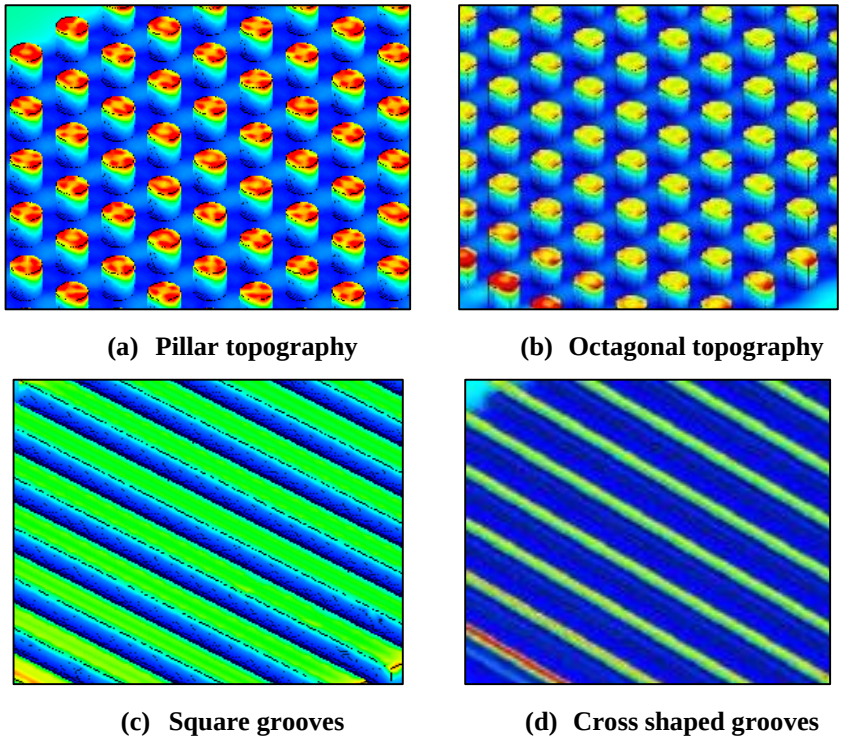

(a) Pillar topography **(b) Octagonal topography**

(c) Square grooves **(d) Cross shaped grooves**

Fig. 8. Wall shear stress contour plot for all four topographies in the isometric view.

The contour plots show that the wall shear stresses are higher at the peaks of all the topographies. Wall shear stresses are lowest near the base of all the topographies. Comparisons between the four topographies show that edges at the peaks of the topographies experience the highest shear stresses. This is most apparent for the pillars and the octagonal topographies.

3.2.1. Average wall shear stress analysis

Figure 9 summarizes the average wall shear stress at the peaks and base of all topographies.

Figure 9 shows a histogram of average wall shear stresses over two separate heights of four different topographies. It can be seen that pillars have the highest average wall shear stress for both peaks and base, followed by octagons, cross shaped grooves and lastly the squared grooves. Average wall shear stress at peaks decreases slightly from pillars to octagons, from octagons to cross shaped grooves and then decreases further for squared grooves. Unlike the peaks, average wall shear stresses at all four topography bases only demonstrate slight differences.

For all topography geometries, the average wall shear stresses at the peaks are at least 42 times greater of that at the base. This is because fluid flows through the peaks at a higher velocity with potentially larger contact area, thus creating higher shear stresses compared to the base and the gaps between topography geometries.

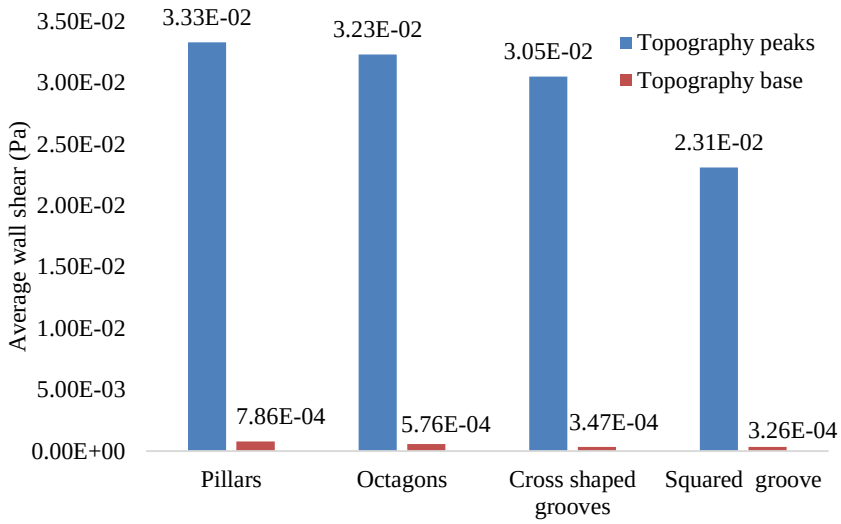

Fig. 9. Average wall shear stresses at peaks and base for the four topographies.

3.3. Overall analysis of results

From Sections 3.1. and 3.2., it is likely that pillars exhibit the best antifouling potential among the four topography geometries. There are several reasons for this. The first is because the formation of vortices in the gaps between pillars (Fig. 6) is among the least amongst the four topographies. The lack of vortices reduces the accumulation of biofouling material. The next reason is that flow at the peaks of pillars are reasonably high among the four topographies. This quick flow amongst the pillars is likely to make it difficult for biofouling organisms to move in a stable manner and explore among the topographies. Without being able to explore, the likelihood of organisms settling on the surface would decrease significantly [12]. Although velocity at the peaks of cross shaped grooves are the highest, this topography is less suitable for antifouling applications because vortices form more consistently (i.e., more biofouling accumulation) for this topography in comparison to the pillars. Pillars also showed the highest average wall shear stresses at both peaks and base in comparison to the other three topographies. The higher the wall shear stresses, the higher the resistance of that topography towards fouling of microorganisms [7]. The topography that is likely to be the least effective at deterring biofouling would be the square grooves. This is demonstrated through the low fluctuations in velocity, lower shear stresses around the topography and the consistent formation of vortices that will accumulate biofouling material instead of removing them.

4. Conclusions

Microtopographies of varied geometries and fixed sizes were assessed numerically in relation to biofouling control. Based on the comparisons of velocity and wall shear stress of the four investigated topographies, it was found that pillars are likely to have the highest antifouling potential. It was also determined that grooves are unfavourable for antifouling purposes because these geometries promotes the

accumulation of biofouling material through the formation of vortices between the grooves. This study also determined that topography peaks, regardless of topography geometries are areas where shear stresses are the greatest and are likely to aid in the shearing off and removal of biofouling materials.

Based on results from this study, future studies should avoid designing topographies that consist of grooves to reduce the formation of vortices. Topographies should also consist of peaks with as many edges as possible. These edges promotes greater shear stresses that will increase the difficulty for organisms to settle on the surface.

Nomenclatures

P	Static pressure, Pa
$S_{m,x}$	Source term for components in the x-direction
$S_{m,y}$	Source term for components in the y-direction
$S_{m,z}$	Source term for components in the z-direction
u	Velocity component in the x-direction, m/s
v	Velocity component in the y-direction, m/s
w	Velocity component in the z-direction, m/s

Greek Symbols

μ	Dynamic Viscosity of fluid material in the fluid domain
ρ	Density of the fluid material in the fluid domain

Abbreviations

CAD	Conputer aided design
CFD	Computational Fluid Dynamics

References

1. Willey, J.M.; Sherwood, L.M.; and Woolverton C.J. (2008). *Prescott, Harley, Klein's Microbiology* (7th ed). New York: Colin Wheatley/Janice Roerig-Blong.
2. Steinhagen, H.M. (2000). *Heat exchanger fouling: mitigation and cleaning technique*. Rugby: Institution of Chemical Engineers,.
3. Chambers, L.D.; Stokes, K.R.; Walsh, F.C.; and Wood, R.J.K. (2006). Modern approaches to marine antifouling coatings. *Surface Coatings Technology*, 201(6), 3642-3652.
4. Ekblad, T. (2010). *Hydrogel coatings for biomedical and biofouling applications*. Thesis. Linköping University, Sweden.
5. Earley, P.J.; Swope, B.L.; Barbeau, K.; Bundy, R.; McDonald, J.A.; and Rivera-Duarte, I. (2014) Life cycle contributions of copper from vessel painting and maintenance activities. *Biofouling*, 30(1), 51-68.
6. Halder, P.; Nasabi, M.; Jayasuriya, N.; Shimeta, J.; Deighton, M.; Bhattacharya, S. (2014) An assessment of the dynamic stability of

microorganisms on patterned surfaces in relation to biofouling control. *Biofouling*, 30(6), 695-707.

7. Myan, F.W.Y.; Walker, J.; and Paramor, O. (2013) The interaction of marine fouling organisms with topography of varied scale and geometry: a review. *Biointerphases*, 8(1), 30.
8. Petronis, Š.; Berntsson, K.; Gold, J.; and Gatenholm, P. (2000) Design and microstructuring of PDMS surfaces for improved marine biofouling resistance. *Journal of Biomaterial Science Polymer Edition*, 11(10), 1051-1072.
9. Won, Y.-J.; Jung, S.-Y.; Jang, J.-H.; Lee, J.-W.; Chae, H.-R.; Choi, D.-C.; Ahn, K.H.; Lee, C.-H.; and Park, P.-K. (2016). Correlation of membrane fouling with topography of patterned membranes for water treatment. *Journal of Membrane Science*, 498, 14-19.
10. Mortensen, N.A.; Okkels, F.; and Bruus, H. (2005). Reexamination of Hagen-Poiseuille flow: Shape dependence of the hydraulic resistance in microchannels. *Physical Review E*, 71(5). 57301.
11. Halder, P.; Nasabi, M.; Lopez, F.J.T.; Jayasuriya, N.; Bhattacharya, S.; Deighton, M.; Mitchell, A.; and Bhuiyan, M. A. (2013). A novel approach to determine the efficacy of patterned surfaces for biofouling control in relation to its microfluidic environment. *Biofouling*, 29(6) 697-713.
12. Myan, F.W.Y. (2017) *The influence of physical attributes of surface topographies in relation to marine biofouling.* Thesis. University of Nottingham Ningbo China, China.